Physics Letters A 382 (2018) 581–587

Contents lists available at ScienceDirect

Physics Letters A

www.elsevier.com/locate/pla

An infinite 3-D quasiperiodic lattice of chaotic attractors

Chunbiao Li [a,b,*], Julien Clinton Sprott [c]

[a] Jiangsu Key Laboratory of Meteorological Observation and Information Processing, Nanjing University of Information Science & Technology, Nanjing 210044, China
[b] Collaborative Innovation Center on Forecast and Evaluation of Meteorological Disasters, Nanjing University of Information Science & Technology, Nanjing 210044, China
[c] Department of Physics, University of Wisconsin-Madison, Madison, WI 53706, USA

ARTICLE INFO

Article history:
Received 27 July 2017
Received in revised form 8 December 2017
Accepted 9 December 2017
Available online 19 December 2017
Communicated by C.R. Doering

Keywords:
Multistability
Infinitely many attractors
Offset boosting

ABSTRACT

A new dynamical system based on Thomas' system is described with infinitely many strange attractors on a 3-D spatial lattice. The mechanism for this multistability is associated with the disturbed offset boosting of sinusoidal functions with different spatial periods. Therefore, the initial condition for offset boosting can trigger a bifurcation, and consequently infinitely many attractors emerge simultaneously. One parameter of the sinusoidal nonlinearity can increase the frequency of the second order derivative of the variables rather than the first order and therefore increase the Lyapunov exponents accordingly. We show examples where the lattice is periodic and where it is quasiperiodic, that latter of which has an infinite variety of attractor types.

1. Introduction

A 3-D cyclically symmetric dynamical system is one whose equations are given by $\dot{x} = f(x, y, z)$, $\dot{y} = f(y, z, x)$, $\dot{z} = f(z, x, y)$, where all the functions are the same except with their variables rotated. Some such systems are known to produce chaos including Halvorsen's system [1] and a piecewise-linear system [2].

Thomas [3] proposed a cyclically symmetric dissipative dynamical system

$$\begin{cases} \dot{x} = \sin(y) - bx, \\ \dot{y} = \sin(z) - by, \\ \dot{z} = \sin(x) - bz, \end{cases} \tag{1}$$

whose linear damping governs the dynamics and controls the dimension of the attractor from 0 to 3 [4–6]. Replacing the linear damping in system (1) by a sinusoidal damping [7,8] and introducing a new parameter a to control the ratio of the two periods gives the system

$$\begin{cases} \dot{x} = \sin(ay) - b\sin(x), \\ \dot{y} = \sin(az) - b\sin(y), \\ \dot{z} = \sin(ax) - b\sin(z). \end{cases} \tag{2}$$

Since all the terms are spatially periodic, the resulting system admits multiple coexisting solutions depending on the initial conditions.

Offset boosting refers to a transformation that can shift any of the variables in a system and hence its attractor in phase space without altering the system solutions [9]. If the periods for all these trigonometric functions are identical ($a = 1$), any attractor will be infinitely reproduced by periodic offset boosting [9–13]. However, if the trigonometric functions have different spatial periods ($a \neq 1$), infinitely many heterogeneous attractors will emerge from different initial conditions as a result of the offset boosting. If the two spatial periods are commensurate (rational a), the lattice of attractors consists of a finite number of attractor types, but if the periods are incommensurate (irrational a), there will be infinitely many types typically consisting of a combination of different strange attractors and limit cycles.

In this paper, a cyclically symmetric system with periodic sinusoidal damping is proposed. Section 2 derives its symmetry and equilibrium points. Section 3 discusses its unique route to chaos. Section 4 describes its special multistability with spatially-periodic chaos and reveals the mechanism for multistability. Section 5 shows an example of spatially-quasiperiodic chaos with infinitely many attractor types. Section 6 shows a case where all the attractors merge into one large unbounded strange attractor. Section 7 shows that similar behavior occurs for different trigonometric functions. Conclusions and discussion are given in the last section.

* Corresponding author at: Jiangsu Key Laboratory of Meteorological Observation and Information Processing, Nanjing University of Information Science & Technology, Nanjing 210044, China.
E-mail addresses: goontry@126.com, chunbiaolee@nuist.edu.cn (C. Li).

https://doi.org/10.1016/j.physleta.2017.12.022
0375-9601/

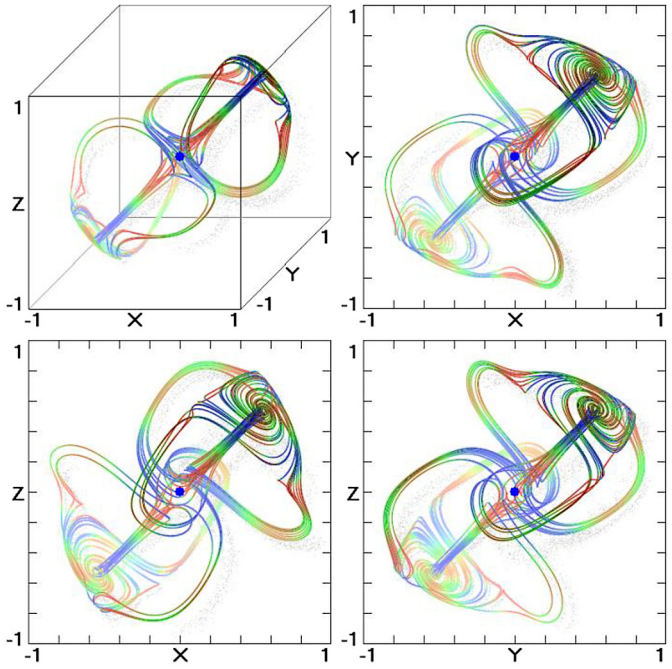

Fig. 1. Chaotic attractor for system (2) with $a = 4.75$, $b = 1$ and initial condition $(0, 1, 0)$. The colors indicate the value of the local largest Lyapunov exponent with positive values in red and negative values in blue. The equilibrium point at the origin is shown as a blue dot. (For interpretation of the references to color in this figure legend, the reader is referred to the web version of this article.)

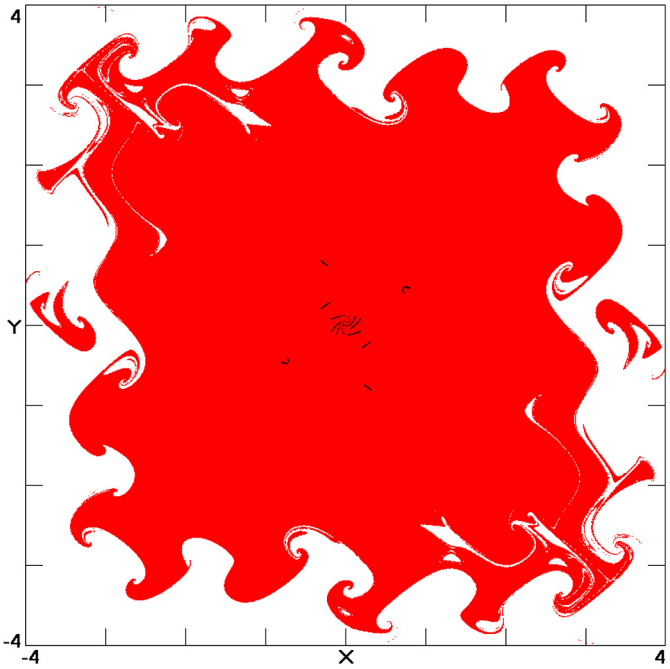

Fig. 2. Basin of attraction of system (2) with $a = 4.75$, $b = 1$ in the plane $z = 0$. The black lines show the cross section of the chaotic attractor in the plane.

2. Symmetry and equilibrium points

System (2) is symmetric about the origin since the transformation of $x \to -x, y \to -y, z \to -z$ gives the same equation and has a periodic rate of volume contraction given by the Lie derivative, $(1/V)dV/dt = \frac{\partial \dot{x}}{\partial x} + \frac{\partial \dot{y}}{\partial y} + \frac{\partial \dot{z}}{\partial z} = -b(\cos(x) + \cos(y) + \cos(z))$. In fact, system (2) is a cyclically symmetric one, where each derivative depends on itself and the other variable, and the functions are all identical except the variables are rotated. The dynamical evolution of the three variables is unified under different initial conditions.

To calculate the equilibrium points, we set $b = 1$ without loss of generality. From $\cos(\frac{ay+x}{2})\sin(\frac{ay-x}{2}) = \cos(\frac{az+y}{2})\sin(\frac{az-y}{2}) = \cos(\frac{ax+z}{2})\sin(\frac{ax-z}{2}) = 0$, eight groups of equilibrium points can be obtained. One group of equilibrium points is $(\frac{2\pi(k_3a^2+k_2a+k_1)}{a^3-1}, \frac{2\pi(k_1a^2+k_3a+k_2)}{a^3-1}, \frac{2\pi(k_2a^2+k_1a+k_3)}{a^3-1})$. For $a \neq 1$, they are related by different combinations of the integers k_i. When $k_1 = k_2 = k_3 = 0$, the eigenvalues are $(a - 1, (-\frac{a}{2} - 1) \pm \frac{\sqrt{3}}{2}ai)$ which implies that the corresponding equilibrium point at the origin is an unstable saddle-focus of index-1 when $a > 1$. There are other equilibrium points of different stability, which will be ignored here because of the complicated forms in the expression of their location and eigenvalues. All these equilibrium points affect their local dynamics giving different attractors.

When $a = 4.75$, $b = 1$, system (2) has a self-excited chaotic attractor near the origin with Lyapunov exponents $(0.2822, 0, -2.9562)$ and a Kaplan–Yorke dimension of 2.0955. The strange attractor is shown in Fig. 1, whose basin of attraction in the plane $z = 0$ is shown in Fig. 2. The projection onto different orthogonal planes (*i.e.*, $x = 0$, $y = 0$) has the same shape since system (2) has cyclical symmetry.

3. Bifurcation and robust chaos

The parameter a in system (2) is a bifurcation parameter, which also influences the offset boosting since it changes the period of the corresponding sinusoidal nonlinearity. To demonstrate this, the Lyapunov exponents, Kaplan–Yorke dimension, and bifurcation diagram for the attractor nearest to the origin are given in Fig. 3, where X_m means the local maximum values of the variable x. There is a Hopf bifurcation for $a = -2$, $b = 1$ where the eigenvalues of the equilibrium point at the origin are $(-3, 0 \pm 1.7321i)$. Unlike other systems [14–21], system (2) has many windows of chaos. For positive values of a below the first such window, most of the limit cycles are asymmetric for the initial condition $(0, 1, 0)$ as shown in Fig. 4; while larger values of a give mostly symmetric limit cycles as shown in Fig. 5. All the attractors shown in Figs. 4 and 5 are for the initial condition $(0, 1, 0)$, and there are infinitely many other attractors for each parameter as shown in the next section. In fact, for the asymmetric case, the system has symmetric pairs of coexisting attractors at many of the lattice sites where the symmetry is broken.

With a further increase in the parameter a, the chaotic solution of system (2) also changes from asymmetric to symmetric and finally retains its chaos with a largest Lyapunov exponent and Kaplan–Yorke dimension that increase with a. As shown in Fig. 6, when $b = 1$, and $a = 4.5$ the attractor is asymmetric; when $b = 1$, $a = 9.5, 10, 12, 18, 50$, the attractor is symmetric, and the second derivative of the variables, which dictates the characteristic frequency of oscillation, increases. Lyapunov exponents and Kaplan–Yorke dimensions of these attractors are shown in Table 1.

This phenomenon is associated with the more closely spaced equilibrium points. Without loss of generality, assume $b = 1$, when the parameter a increases, system (2) has more closely spaced equilibrium points. Since $\dot{x} = \sin(ay) - \sin(x) \in [-2, 2]$, the derivative of the variable x (if a variable corresponds to the displacement of an object, the derivative of that variable corresponds to the velocity) cannot be increased without limit. But when a second derivative is taken, giving the equation $\ddot{x} = a\cos(ay)(\sin(az) - \sin(y)) - \cos(x)(\sin(ay) - \sin(x)) \in [-2(|a| + 1), 2(|a| + 1)]$, the displacement in the x direction has a continuously increasing acceleration (within a limited range of amplitudes). The corresponding strange attractors and their frequency spectra are shown in Fig. 7

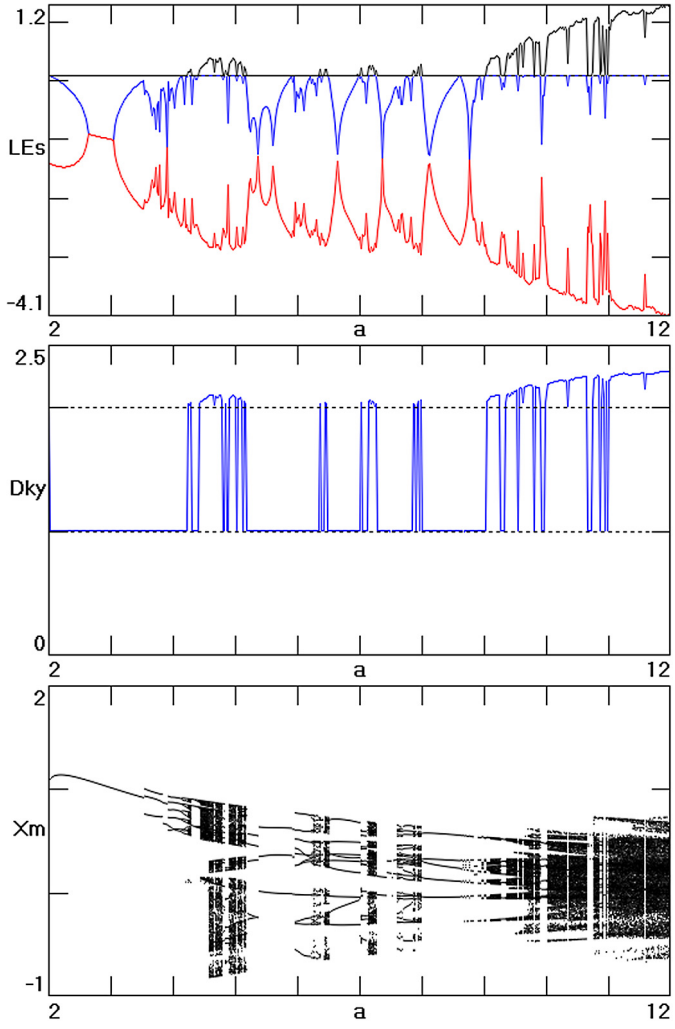

Fig. 3. Dynamical behavior of system (2) with initial condition $(0, 1, 0)$ when a varies in [2,12] for $b = 1$ showing Lyapunov exponents, Kaplan–Yorke dimension, and bifurcation diagram.

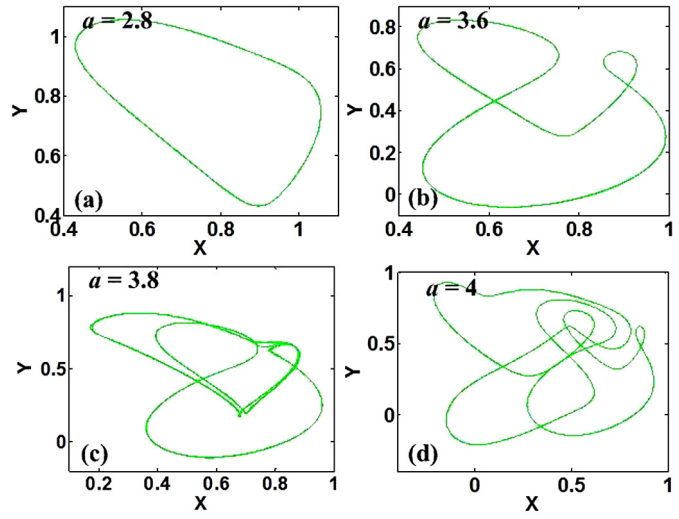

Fig. 4. Typical asymmetric limit cycles of system (2) with initial conditions $(0, 1, 0)$ and $b = 1$ below the first window of chaos.

for larger values of a. The range of the variables becomes smaller thereby compressing the attractor, while the characteristic frequencies increase along with the Lyapunov exponent [22,23].

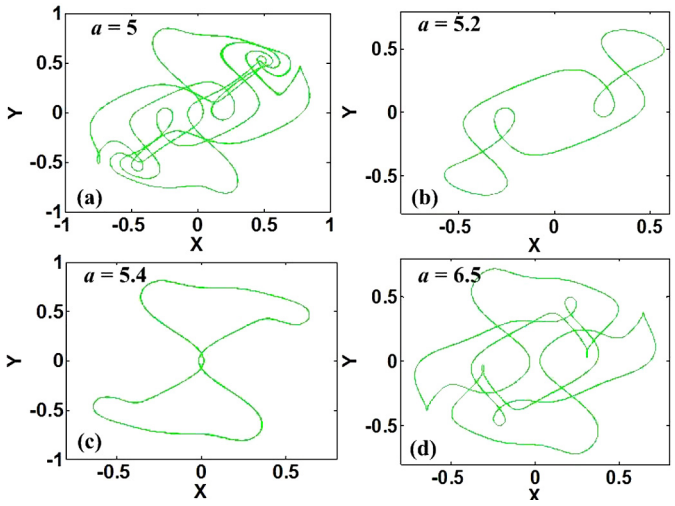

Fig. 5. Typical symmetric limit cycles of system (2) with initial conditions $(0, 1, 0)$ and $b = 1$ above the first window of chaos.

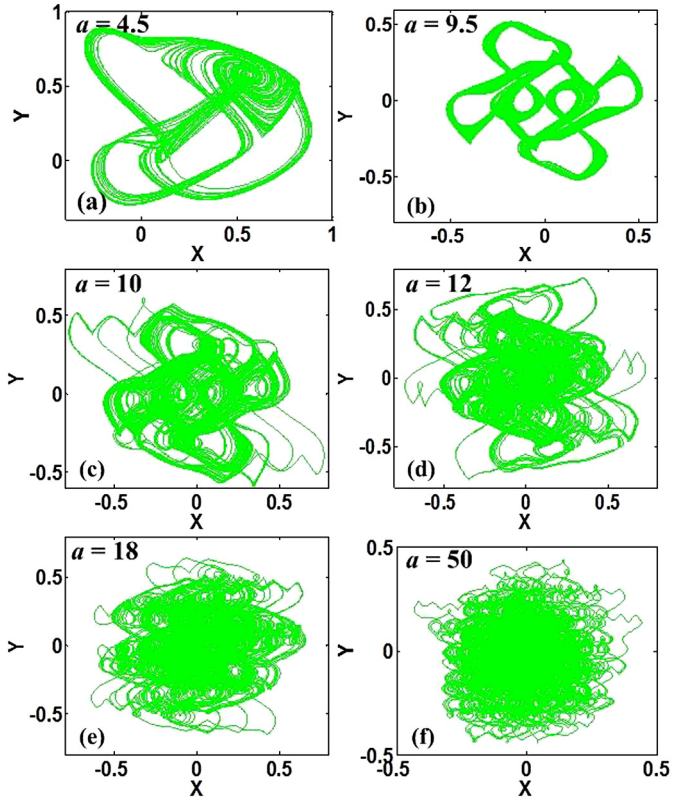

Fig. 6. Chaotic attractor of system (2) with initial conditions $(0, 1, 0)$ and $b = 1$.

Table 1
Lyapunov exponents and Kaplan–Yorke dimensions of the strange attractors for various a in system (2) with $b = 1$ and initial conditions $(0, 1, 0)$.

Parameter	Lyapunov exponents (LEs)	Kaplan–Yorke dimension (D_{ky})
$a = 4.5$	0.1809, 0, −2.8216	2.0641
$a = 9.5$	0.4459, 0, −3.3607	2.1327
$a = 10$	0.3901, 0, −3.3068	2.1180
$a = 12$	1.1607, 0, −4.0652	2.2855
$a = 18$	2.3259, 0, −5.2471	2.4433
$a = 50$	7.2548, 0, −10.2305	2.7091

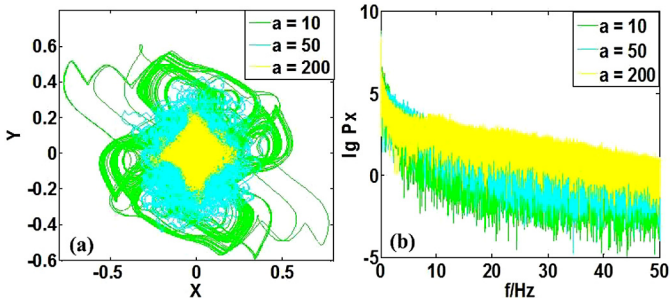

Fig. 7. Chaotic oscillation from system (2) with initial conditions $(0, 1, 0)$ and $b = 1$ (a) strange attractor, (b) corresponding frequency spectrum.

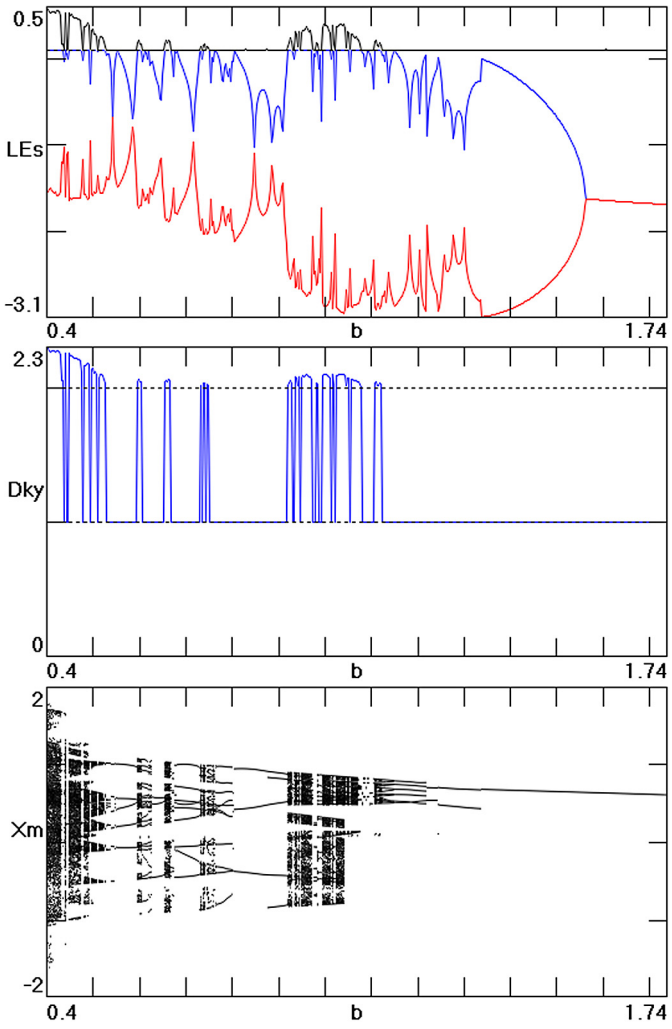

Fig. 8. Dynamical behavior of system (2) with initial conditions $(0, 1, 0)$ when b varies in $[0.4, 1.74]$ at $a = 4.75$ including Lyapunov exponents, Kaplan–Yorke dimension, and bifurcation diagram.

When $a = 4.75$ and b varies in $[0.4, 1.74]$, the diagrams of bifurcation and Lyapunov exponent spectrum are as given in Fig. 8. In contrast to the system with a varying parameter a, this figure shows that the parameter b alters the dynamics of system (2) dramatically, giving an inverse period-doubling progressing from chaos to a stable equilibrium and with numerous periodic windows. For $b < 0.4$, system (2) has an unbounded strange attractor that will be described later.

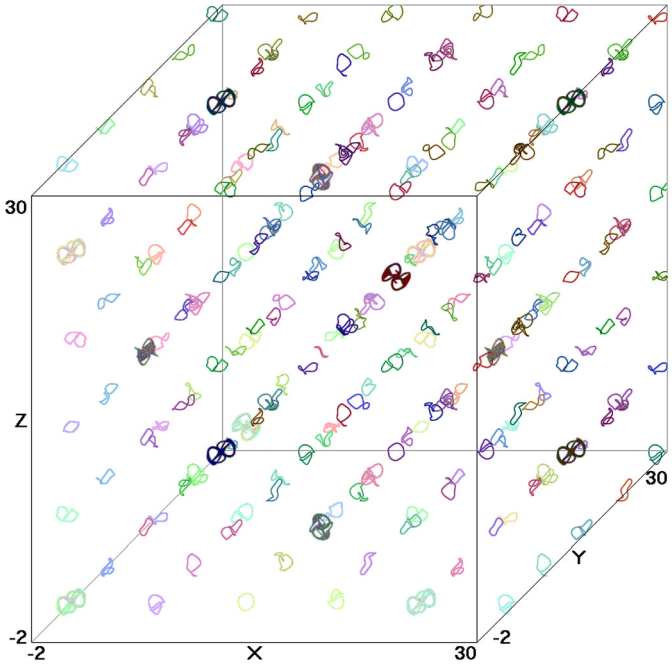

Fig. 9. Coexisting attractors of system (2) with $a = 4.75$, $b = 1$.

4. Infinite periodic lattice of attractors

The multistability of a dynamical system relates to its initial conditions. The mechanism responsible for multistability is associated with offset boosting and atypical bifurcation. To show this, replace the variable x with $x+c$, correspondingly $\sin(x)$ and $\sin(ax)$ become $\sin(x+c)$ and $\sin(a(x+c))$, indicating that the bifurcation parameter a becomes entangled with the offset parameter c. In fact, an offset in any of the variables will introduce two constants in the right-hand side of Eq. (2), and therefore it will influence the dynamical behavior. For $x \to x+c$, system (2) becomes

$$\begin{cases} \dot{x} = \sin(ay) - b\sin(x+c), \\ \dot{y} = \sin(az) - b\sin(y), \\ \dot{z} = \sin\big(a(x+c)\big) - b\sin(z). \end{cases} \tag{3}$$

Because it has two different periods, 2π and $2\pi/a$, the bifurcation parameter a in system (3) becomes entangled with the offset boosting parameter c. System (2) can thus produce an infinite 3-D lattice of attractors, with a mixture of chaos and limit cycles. Amplitude control provides a way to find coexisting attractors [24,25]. The above analysis also shows that offset boosting with a fixed initial condition gives a method for identifying multistability [9].

As predicted, when $a = 4.75$, $b = 1$, there are limit cycles coexisting with strange attractors as shown in Fig. 9. The colors are arbitrary and are used only to distinguish attractors that might otherwise overlap in a given projection. The basins of attraction for one row of the coexisting attractors in the $z = 0$ plane as shown in Fig. 10 shows the offset separated structure with complicated basin boundaries. The basin structure repeats in the y and z directions. Some periodic attractors are intermingled with the offset-boosted strange attractors, which is caused by the different characteristic lengths and initial conditions.

Besides the new introduced periodic solutions, offsetting of the variable x modulo 2π is obtained for the sinusoidal nonlinearities. Fig. 11 shows that a change in the initial condition x_0 produces not only an offset boosting but also coexisting chaos and limit cycles. Of those nine attractors, three are chaotic, and six are limit cycles. As shown in Fig. 9, the initial conditions of the variables x, y, and

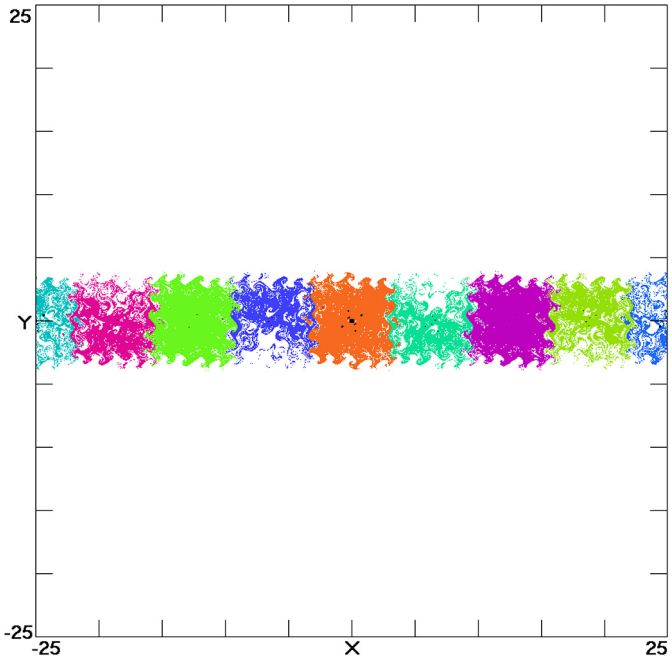

Fig. 10. Basins of attraction for one row of coexisting attractors when $z = 0$.

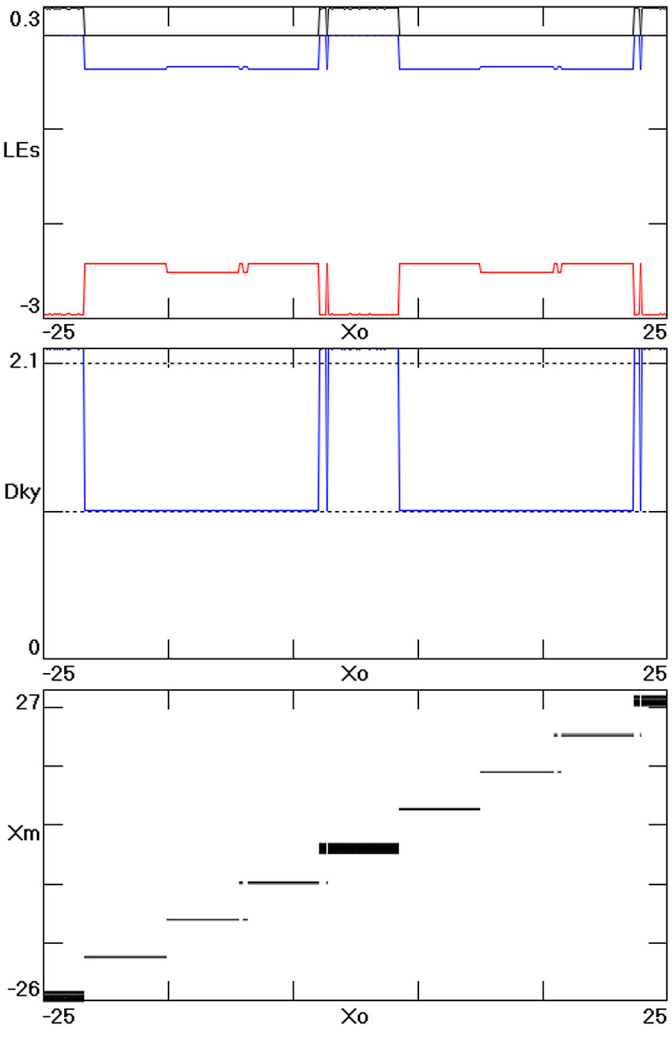

Fig. 11. Dynamical behavior of system (2) with $a = 4.75$ and $b = 1$ when the initial condition x_0 varies in $[-25, 25]$ for $y_0 = 1$, $z_0 = 0$.

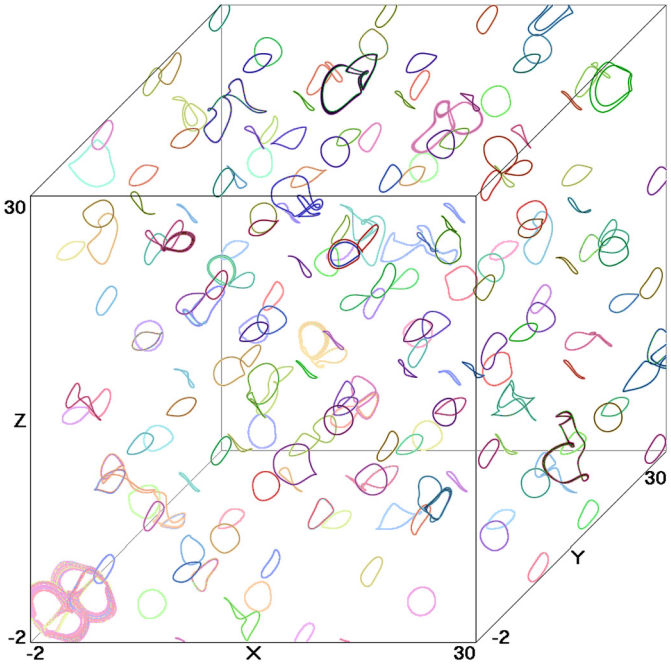

Fig. 12. Typical coexisting attractors of system (2) with $a = (\sqrt{5}+1)/2$, $b = 0.7$.

z have the same effect on system (2), giving the same attractors that hop between chaos and periodicity.

Since $a = 4.75 = 19/4$ is a rational number, the 3-D lattice is spatially periodic with a period of $4 \times 2\pi$, and thus a cube of size 8π in each direction will contain 64 coexisting attractors, and there are infinitely many such identical cubes. Some of the cells contain a symmetric pair of attractors. Many of the attractors have identical properties except for a rotation by 90 degrees as a result of the cyclical symmetry. Further analysis of the 64 attractors using the average trace of their Jacobian matrix to distinguish among them shows that of the 64 attractors in each cube, only five are unique. The spatial pattern of the five is complicated and nonobvious. As a practical matter, it is necessary to avoid initial conditions that lie at exact multiples of 2π to break the symmetry of the three variables. Note that there are many more equilibrium points than there are attractors and most of the equilibria are saddle-focus pairs of index-1 and index-2 with occasional saddle nodes.

5. Infinite quasiperiodic lattice of attractors

To produce an infinite lattice containing an infinite variety of attractors, it is necessary to choose an irrational value for a. For that purpose we take $a = (\sqrt{5}+1)/2$ (the golden mean) and choose $b = 0.7$ to make the attractor closest to the origin chaotic. Fig. 12 shows a representative cube along with the attractors that it contains. There are degeneracies due to the inversion symmetry (change of sign of the variables) and the cyclical symmetry (90 degree rotations), but there are infinitely many attractors with different values of the trace of their Jacobian. Most of these attractors are limit cycles, but some are strange attractors. There is also an infinite variety of equilibrium points, but they are all saddle foci with a similar number of index-1 and index-2.

6. Unbounded strange attractor

Fig. 13 shows that the attractor in the vicinity of the origin for the quasiperiodic lattice is chaotic only over a narrow range of b in the vicinity of 0.7 and that the more typical attractor is a limit cycle. However, when b decreases to about 0.32, the limit cycle at the origin merges with a nearby limit cycle to form a

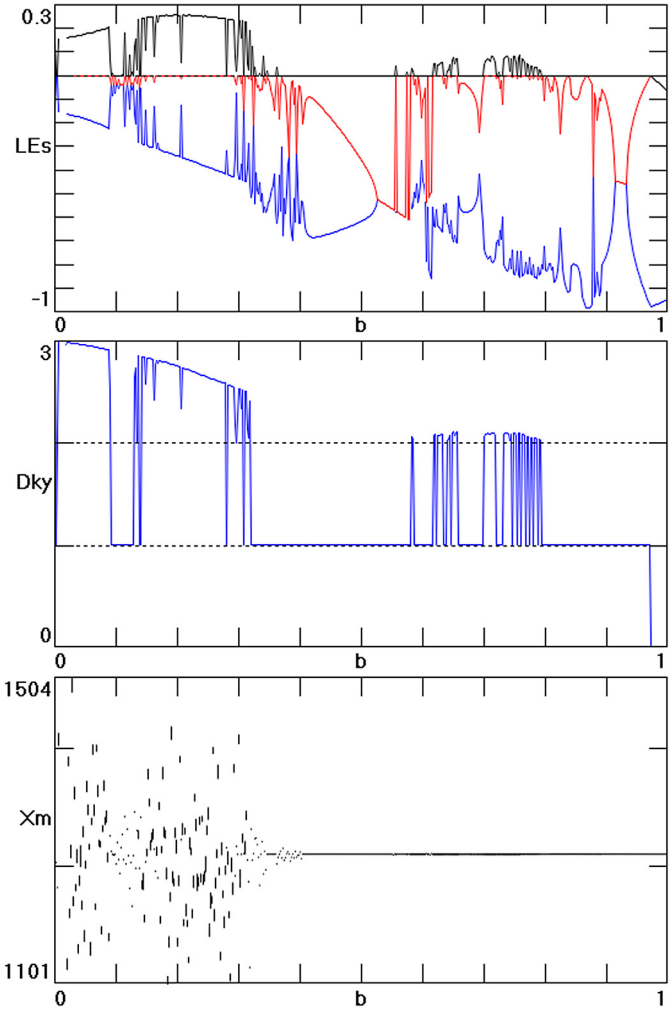

Fig. 13. Dynamical behavior of system (2) with initial conditions $(0, 1, 0)$ when b varies in $[0, 1]$ at $a = (\sqrt{5}+1)/2$ including Lyapunov exponents, Kaplan–Yorke dimension and bifurcation diagram.

larger limit cycle that then merges with others, eventually forming a single large strange attractor that is unbounded for $b = 0.2$ with Lyapunov exponents $(0.257, 0, -0.341)$ and a Kaplan–Yorke dimension of 2.752, a typical piece of which is shown in Fig. 14. Thus the system exhibits a kind of fractional Brownian motion. However, since the Kaplan–Yorke dimension is less than 3.0, the orbit is a set of measure zero in the space.

When b decreases further to 0.1, there is a very long chaotic transient where the orbit wanders throughout the lattice, but it eventually finds a stable limit cycle embedded in one of the cells as shown in Fig. 15. This is just one of an infinite number of such embedded limit cycles, but they are rare.

7. Other periodic functions

The sine terms in system (2) can be replaced by other periodic functions giving behavior similar to that described above. For example, the system

$$\begin{cases} \dot{x} = \sin(ay) - b\tan(x), \\ \dot{y} = \sin(az) - b\tan(y), \\ \dot{z} = \sin(ax) - b\tan(z) \end{cases} \tag{4}$$

can also give an infinite 3-D lattice of attractors. Specifically, when $a = 4.75$, $b = 0.7$, it has a chaotic solution with Lyapunov exponents $(0.1650, 0, -2.9213)$ and a Kaplan–Yorke dimension of

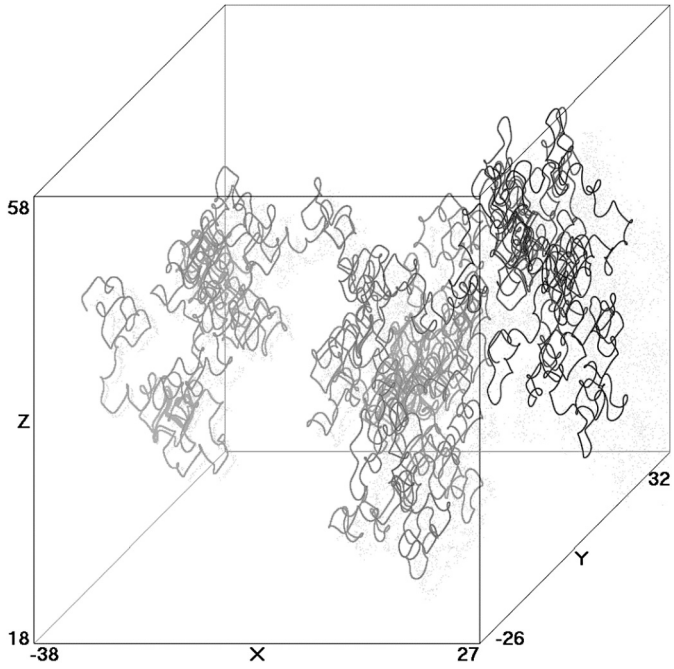

Fig. 14. Unbounded strange attractor of system (2) with $a = (\sqrt{5}+1)/2$, $b = 0.2$ for initial conditions $(10, 15, 31)$.

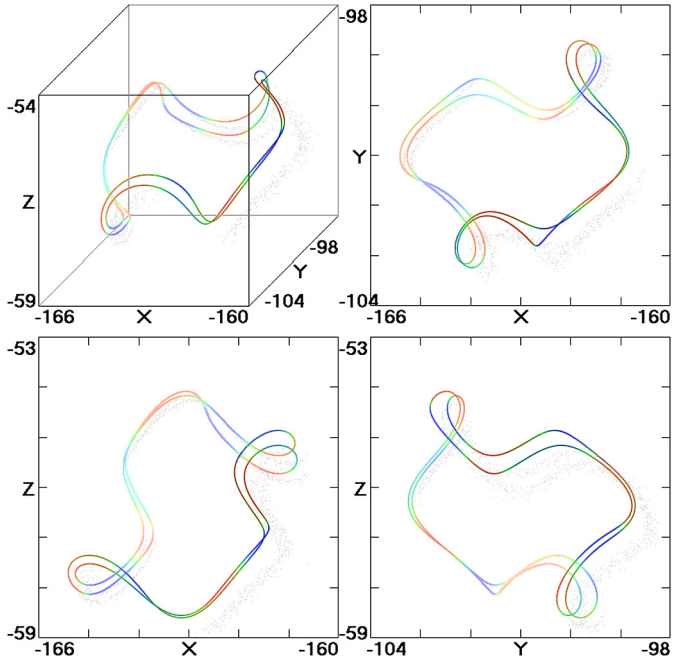

Fig. 15. A stable limit cycle embedded in one of the cells for system (2) with $a = (\sqrt{5}+1)/2$, $b = 0.1$.

2.0565 for the initial conditions $(0, 1, 0)$. The kinds of coexisting attractors are as shown in Fig. 16. Comparing Fig. 16 with Fig. 9 and Fig. 12 shows that the number of coexisting attractors in the same cube is greater in this case since it has two different periods, π and $2\pi/a$.

8. Conclusions and discussion

Multistability has attracted great attention for its value and problems in engineering design. However, the mechanisms for different regimes of coexisting attractors have not been sufficiently revealed. Some symmetric systems have coexisting attractors when

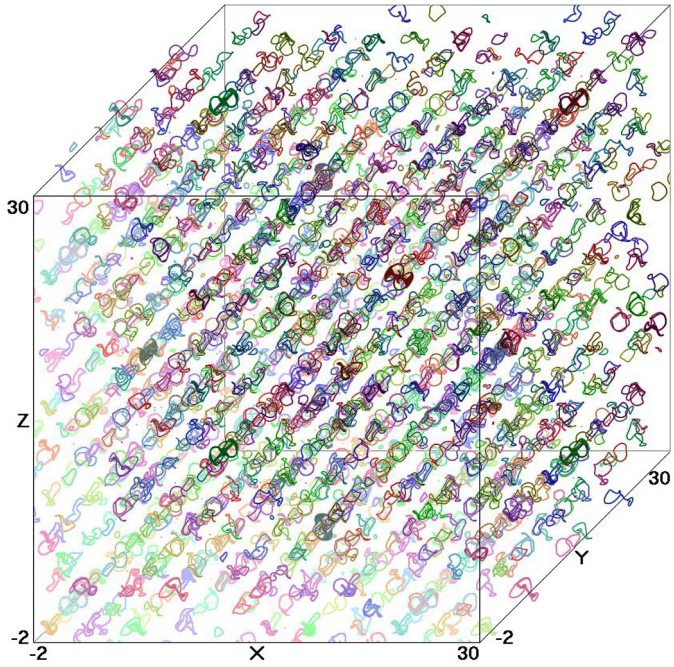

Fig. 16. Coexisting attractors of system (4) with tangent damping for $a = 4.75$, $b = 0.7$.

the symmetry is broken [26–28], some systems with hidden attractors show multistability for the equilibrium points [29–31], and extreme multistability is associated with extraneous dimensions [32–34]. However, offset boosting provides a new mechanism for producing infinitely many attractors. Unbalanced offset boosting in the same variable can generate different types of coexisting attractors.

By introducing spatially sinusoidal damping in Thomas' system, an infinite 3-D lattice of coexisting attractors consisting of symmetric and asymmetric limit cycles and strange attractors is produced. Increasing the spatial frequency of the sinusoidal function causes the system to contain more closely spaced equilibrium points and correspondingly produces chaotic attractors with larger Lyapunov exponents. The mechanism for producing infinitely many attractors is rooted in offset boosting and spatially-periodic trigonometric nonlinearities.

Acknowledgements

This work was supported financially by the Natural Science Foundation of the Higher Education Institutions of Jiangsu Province (Grant No. 16KJB120004), the Startup Foundation for Introducing Talent of NUIST (Grant No. 2016205), the National Natural Science Foundation of China (Grant No. 61401198) and a Project Funded by the Priority Academic Program Development of Jiangsu Higher Education Institutions.

References

[1] J.C. Sprott, Chaos and Time-Series Analysis, Oxford University Press, Oxford, 2003.
[2] J.C. Sprott, Elegant Chaos: Algebraically Simple Chaotic Flows, World Scientific, Singapore, 2010.
[3] R. Thomas, Int. J. Bifurc. Chaos Appl. Sci. Eng. 9 (1999) 1889.
[4] J.C. Sprott, K.E. Chlouverakis, Int. J. Bifurc. Chaos Appl. Sci. Eng. 17 (2007) 2097.
[5] K.E. Chlouverakis, J.C. Sprott, Chaos 17 (2007) 023110.
[6] B. Munmuangsaen, J.C. Sprott, W.J. Thio, A. Burcarino, L. Fortuna, Int. J. Bifurc. Chaos Appl. Sci. Eng. 25 (2015) 1530036.
[7] E. Kaslik, S. Sivasundaram, in: Proceedings of the International Joint Conference on Neural Networks, IEEE Computer Society Press, San Jose, California, USA, 2011.
[8] E. Kaslik, S. Sivasundaram, Neural Netw. 32 (2012) 245.
[9] C. Li, X. Wang, G. Chen, Nonlinear Dyn. (2017), https://doi.org/10.1007/s11071-017-3729-1.
[10] C. Li, J.C. Sprott, Y. Mei, Nonlinear Dyn. 89 (2017) 2629.
[11] C. Li, J.C. Sprott, H. Xing, Phys. Lett. A 380 (2016) 1172.
[12] C. Li, J.C. Sprott, W. Hu, Y. Xu, Int. J. Bifurc. Chaos Appl. Sci. Eng. 27 (2017) 1750160.
[13] C. Li, J.C. Sprott, Optik 127 (2016) 10389.
[14] Z. Wei, I. Moroz, A. Liu, Turk. J. Math. 38 (2014) 672.
[15] Z. Wei, R. Wang, A. Liu, Math. Comput. Simul. 100 (2014) 13.
[16] S. He, K. Sun, S. Banerjee, Eur. Phys. J. Plus 131 (2016) 1.
[17] J. Mou, K. Sun, J. Ruan, S. He, Nonlinear Dyn. 86 (2016) 1735.
[18] S. He, K. Sun, H. Wang, Physica A 461 (2016) 812.
[19] H. Jiang, Q. Bi, Nonlinear Dyn. 67 (2012) 781.
[20] J.C. Sprott, Eur. Phys. J. Spec. Top. 224 (2015) 1409.
[21] M. Molaie, S. Jafari, J.C. Sprott, S.M.R.H. Golpayegani, Int. J. Bifurc. Chaos Appl. Sci. Eng. 23 (2013) 1350188.
[22] C. Li, J.C. Sprott, Z. Yuan, H. Li, Int. J. Bifurc. Chaos Appl. Sci. Eng. 24 (2015) 1450131.
[23] W. Hu, A. Akgul, C. Li, T. Zheng, P. Li, J. Circuits Syst. Comput. 26 (2017) 1750158.
[24] C. Li, J.C. Sprott, Nonlinear Dyn. 78 (2014) 2059.
[25] C. Li, J.C. Sprott, H. Xing, Int. J. Bifurc. Chaos Appl. Sci. Eng. 26 (2016) 1650233.
[26] C. Li, W. Hu, J.C. Sprott, X. Wang, Eur. Phys. J. Spec. Top. 224 (2015) 1493.
[27] Q. Lai, S. Chen, Optik 127 (2016) 3000.
[28] B. Bao, Q. Li, N. Wang, Q. Xu, Chaos 26 (2016) 043111.
[29] J.C. Sprott, X. Wang, G. Chen, Int. J. Bifurc. Chaos Appl. Sci. Eng. 23 (2013) 1350093.
[30] Z. Wei, R. Wang, A. Liu, Math. Comput. Simul. 100 (2014) 13.
[31] S. Jafari, J.C. Sprott, F. Nazarimehr, Eur. Phys. J. Spec. Top. 224 (2015) 1469.
[32] C.R. Hens, R. Banerjee, U. Feudel, S.K. Dana, Phys. Rev. E 85 (2012) 035202R.
[33] M.S. Patel, U. Patel, A. Sen, G.C. Sethia, C. Hens, S.K. Dana, U. Feudel, K. Showalter, C.N. Ngonghala, R.E. Amritkar, Phys. Rev. E 89 (2014) 022918.
[34] J.C. Sprott, C. Li, Phys. Rev. E 89 (2014) 066901.